Solar Energy 163 (2018) 537–544

Contents lists available at ScienceDirect

Solar Energy

journal homepage: www.elsevier.com/locate/solener

The colour rendering index and correlated colour temperature of dye-sensitized solar cell for adaptive glazing application

Aritra Ghosh*, Prabhu Selvaraj, Senthilarasu Sundaram, Tapas K. Mallick*

Environment and Sustainability Institute (ESI), University of Exeter, Penryn Campus, TR10 9FE, United Kingdom

ARTICLE INFO

Keywords:
Adaptive
DSSC
Glazing
CCT
CRI

ABSTRACT

The colour rendering index (CRI) and correlated colour temperature (CCT) of transmitted daylight through a DSSC glazing is an essential parameter for building interior space comfort. Six small-scale dye-sensitized solar cells (DSSCs) were fabricated by varying TiO_2 electrode thickness, which offered luminous transmittance between 0.19 and 0.53. Below 0.5 transmittance, the CRI for this TiO_2 electrode based DSSC glazing was less than 80. A strong linear correlation was found between CCT and CRI. The CRI of 53% transparent DSSC glazing had only 2.7% lower CRI than 77% transparent double glazing and 72% transparent vacuum glazing.

1. Introduction

Buildings consume 40% of energy worldwide due to heating, cooling and lighting (Sudan et al., 2015; Sudan and Tiwari, 2016, 2014) load demand (Al Dakheel and Tabet Aoul, 2017; Hee et al., 2015). Mitigation of this energy demand is possible by introducing new zero energy building or retrofits the building envelope using energy efficient material. Windows are the weakest part of a building as it allows 40% of total building energy losses. Thus, replacing of low energy efficient window with smart, energy efficient, adaptive glazing is essential (Ghosh, 2014; Ghosh et al., 2017a, 2017b; Ghosh and Norton, 2017a). Moreover, for retrofit application, replacement of windows is easier than any other part of the building (Ghosh et al., 2016a, 2015).

Currently adaptive glazing systems are in research interest for building window applications as they have potential of lighting demand reduction of building and introduce comfortable daylight into space (Jelle et al., 2012; Rezaei et al., 2017; Skandalos and Karamanis, 2015). These glazing systems are mainly switchable (Ghosh et al., 2018a, 2018b; Ghosh and Mallick, 2018) and non-switchable (Ghosh et al., 2016b, 2016c; Ghosh et al., 2018b). Switchable has potential to change its transparency based on occupant demand and comfort (Ghosh et al., 2016). However, for large-scale application this electrically switchable glazing can increase the building switching energy demand (Ghosh et al., 2016d). Photovoltaic (PV) glazing is advantageous over any other smart adaptive glazing as they can control energy losses and generate clean energy (Cuce, 2016; Ng and Mithraratne, 2014; Skandalos and Karamanis, 2015).

In a PV glazing, PV devices are sandwiched between two glass panes (Cuce, 2016; Favoino et al., 2015). These devices can be crystalline silicon (Si) (Park et al., 2010), amorphous Si (Miyazaki et al., 2005), CIGS (Wei et al., 2014), CdTe (Shen et al., 2016), perovskite (Cannavale et al., 2017) or dye-sensitized type solar cells (DSSC) (Kang et al., 2013; Yoon et al., 2011). Compared to other type of PV cells, DSSCs have below attributes, which make them advantageous

- DSSCs are insensitive to environment contaminants, which offer them to prepare under ambient temperature. Thus, easier fabrication process can be adopted such as roll-to-roll, which involves continuous, low-cost manufacturing method to print dye-sensitized solar cells on flexible substrates (Gong et al., 2017, 2012; Grätzel, 2003).
- DSSCs work even in low light conditions. Thus for northern latitude area where diffuse sun lights are majority over direct sunlight, DSSC based windows are excellent choice for building applications (Gong et al., 2017, 2012; Grätzel, 2003; Sharma et al., 2017; Upadhyaya et al., 2013).
- DSSCs are superior than a-Si:H based PV as the transparency can be increased by making use of highly transparent photoanodes and

* Corresponding authors.
E-mail addresses: a.ghosh@exeter.ac.uk (A. Ghosh), t.k.mallick@exeter.ac.uk (T.K. Mallick).

https://doi.org/10.1016/j.solener.2018.02.021
Received 17 May 2017; Received in revised form 5 February 2018; Accepted 7 February 2018
Available online 13 March 2018

Nomenclature

CIE	Commission Internationale de l'Eclairage
CCT	correlated color temperature
CRI	colour rendering index
D65	CIE standard illuminant
ΔE_i	color difference between the color coordinates determined for the same test color samples illuminated by test and the reference illuminants
i	number of test color
R_i	special color rendering index
u_t, v_t	user coordinates system (UCS) or trichromatic coordinate for test illuminant
$W_{t,i}$, $U_{t,i}$, $V_{t,i}$	UCS chromaticity coordinates of test color samples under test illuminant
$W_{r,i}$, $U_{r,i}$, $V_{r,i}$	UCS chromaticity coordinates of test color samples under reference illuminant
X, Y, Z	CIE tristimulus values of test color samples
x, y	chromacity coordinates of test illuminant
$\bar{x}(\lambda),\bar{y}(\lambda),\bar{z}(\lambda)$	color matching functions of 1931 CIE 2°standard observer

counter electrodes. Selecting proper dyes for these devices can provide low eye sensitive factor (Kumara et al., 2017; Richhariya et al., 2017; Shalini et al., 2015).

- DSSCs have positive temperature effect (Berginc et al., 2007; Parisi et al., 2017).

DSSCs were first reported by O'Regan and Grätzel in 1991 (O'Regan and Gratzel, 1991) and the maximum efficiency of 13% was recorded in 2014 (Mathew et al., 2014). The recent progress of DSSC offers it to consider for glazing applications. Fig. 1 shows the different components of a typical liquid electrolyte DSSC for glazing application.

First ever DSSC glazing was fabricated by series connected 9 unit ($80 \times 80\,mm^2$ active area) solar cells which offered 60% average transmission between 500 and 900 nm (Kang et al., 2003). Thermal and optical characteristics of double glazed DSSC window were investigated using WINDOW software where DSSCs were fabricated using green (33% transparent) and red (28% transparent) dyes (Kang et al., 2013). This glazing was able to reduce 60% entering solar heat gain. In an another work, thermal, optical and electrical performance of DSSCs inside a patented glass block were also investigated using COMSOL Multiphysics, WINDOW and Zemax (Morini and Corrao, 2017).

Spectral power distribution (SPD) of solar radiation in the visible range of 380–780 nm is considered as daylight. SPD of natural daylight changes with local latitude, weather, season, time of day, air bound dust and pollutant (Ghosh and Norton, 2017b). SPD of transmitted light into the interior of a room influence the visual comfort and color perception. Glazing transparency, thickness, solar heat gain coefficient and overall heat transfer coefficient are the most common investigated parameters while color properties such as correlated color temperature (CCT) and color rendering index (CRI) evaluations are often overlooked. Colour of transmitted daylight through glazing is an influential factor on indoor comfort. Correlated color temperature (CCT) and color rendering index (CRI) are the two major components to understand the SPD of transmitted light through glazing (Davis and Grinthner, 1990; Luo, 2011). CCT and CRI are the most aesthetic criteria as they show whether the spectrum coming inside through the glazing is suitable for occupant or cross the comfort level. They are used to characterize the illumination quality of white light (D'Andrade and Forrest, 2004). Good quality lighting is an important feature, as the quantity and quality of lights are required for wellbeing, health, interpersonal relationships and aesthetic taste (Bommel and Beld, 2004; Webb, 2006). CRI of a glazing indicates the color of entering daylight into an interior before and after placing a glazing. CRI values can be from 0 to 100 (Gunde et al., 2005) where between 80 and 90 are considered to be acceptable (Chain et al., 2001). CRI close to 100-represents true color perception inside the building, thus, indicates perfect visual quality (Gong et al., 2005; Niu et al., 2006). A CCT needs to be equivalent to that of a blackbody source at temperatures between 3000 and 7500 K (Hernández-Andrés et al., 1999). CCT offers to understand whether light is neutral, bluish white or reddish white. CCT for various daylight sources are listed in Table 1.

CCT and CRI evaluation for PV glazing is rare. CRI for semi-transparent PV module using a-Si PV cells was the only reported work of PV glazing (Lynn et al., 2012). No CCT values were calculated for this type of glazing.

The spectrum of transmitted daylight into an interior space changes due to the presence of DSSC glazing. CRI and CCT characterization of DSSC glazing is required as these parameters assess human response to colors (Ghosh and Norton, 2017b).

In this work, different thickness of DSSCs was realized to evaluate luminous transmittance, CCT and CRI for the incoming daylight through DSSC glazing. CCT and CRI of DSSC glazing were compared with air filled double pane glazing and evacuated (vacuum) glazing.

2. Experiment

2.1. DSSC manufacturing

Six different titanium dioxide (TiO_2) layers (as listed in Table 2) were prepared for DSSCs using screen-printing method in order to measure its solar to electrical efficiency and thermo-optical properties for glazing applications at our solar energy lab, University of Exeter. The thickness of the TiO_2 electrodes was measured using Dektak 8

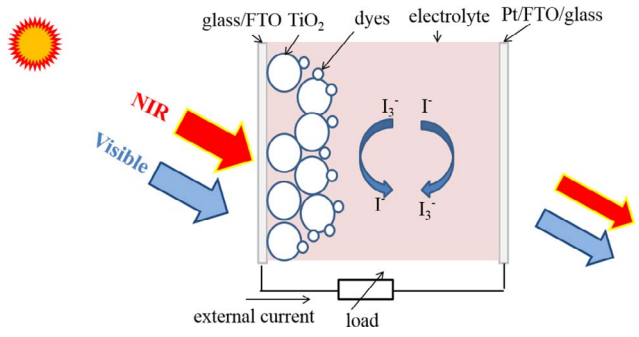

Fig. 1. Schematic illustration of a DSSC glazing. Entering visible light can be changed by tuning TiO_2 thickness, dyes and electrolyte.

Table 1
Correlated color temperatures for various daylight sources of Washington DC USA (Mardaljevic, 2014).

Daylight source	CCT
Sunlight – sunrise or sunset	2000 K
Sunlight – one Hour After Sunrise	3500 K
Sunlight – early Morning	4300 K
Sunlight – late Afternoon	4300 K
Overcast sky	6000 K
Summer skylight	9500–30,000 K

Advanced Development Profiler. Prepared TiO_2 electrode was placed on top of platinum counter electrode to make sandwich type DSSCs. The working electrodes and the corresponding devices were prepared according to the (Ito et al., 2008; Senthilarasu et al., 2012).

Steps involved are shown in the flow-diagram:

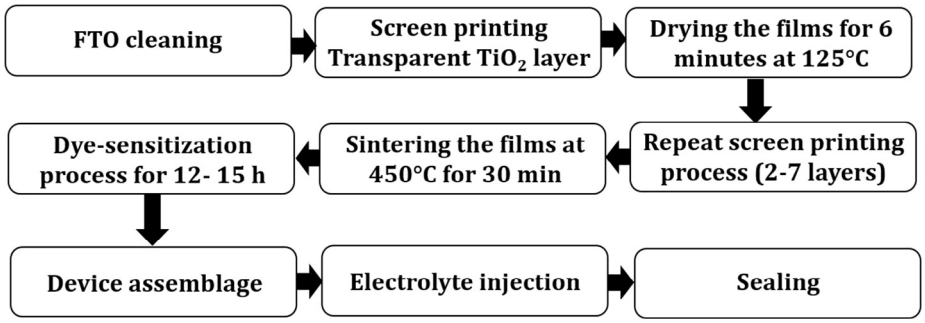

Fig. 2 shows six fabricated DSSCs for glazing applications. Solar to electrical conversion efficiency was measured using indoor solar simulator and I-V tracer. To achieve different transparency of DSSCs, electrode thickness was varied as shown in Table 2.

2.2. Spectrometer measurement & luminous transmission calculation

The transparency of the devices was measured using a UV–VIS–NIR spectrometer (PerkinElmer, Lambda 1050) which provides highly precise transmittance. Transmittance was measured at a step of 1 nm in a wavelength range between 380 nm and 780 nm. The color rendering properties of a glazing were calculated from the spectra measured by a UV–Vis–NIR spectrophotometer.

Luminous transmittance values τ_v are given by (En, 2001)

$$\tau_v = \frac{\sum_{380\,nm}^{780\,nm} D_{65}(\lambda)V(\lambda)\tau(\lambda)\Delta\lambda}{\sum_{380\,nm}^{780\,nm} D_{65}(\lambda)V(\lambda)\Delta\lambda} \quad (1)$$

where $\tau(\lambda)$ is the spectral transmittance of DSSC glazing, D65(λ) is the spectral power distribution of CIE standard illuminant D65, V(λ) is the photopic luminous efficiency function of the human eye and $\Delta\lambda = 10$ nm. Fig. 3 shows the photopic eye sensitivity to light wavelength. The maximum sensitivity is in the green spectral range at 555 nm, where V (λ) has a value of unity, i.e. V (555 nm) = 1.

3. Evaluation of CRI and CCT

To evaluate color properties of the DSSC glazing, method recommended by CIE 13.3-1995 was followed. Color is perception and not possible to measure with any equipment (Lynn et al., 2012). At first CCT was calculated. Color matching functions corresponding to sensitivity of human eye and spectral power distribution of the wavelength dependent transmitted light were used to identify the CCT. For color rendering index evaluation, 1931 CIE chromaticity coordinates of test color samples were evaluated followed by determination of 1964 CIE UCS chromaticity coordinates ($W_{t,i}^*$; $U_{t,i}^*$; $V_{t,i}^*$). Resultant color shift was investigated to find out special color rendering index (R_i) which offered general color rendering index (CRI). All calculations were processed using MATLAB 8.5.

Step 1 for CCT evaluation: The tristimulus values X, Y, Z indicate the three color perception of human eye response. They also indicate how much red, blue and green are in the color. This XYZ color system was established in 1931 and referred as 1931 2°CIE standard observer (CIE 15, 2004; CIE Publication, 1988). Tristimulus values X, Y and Z of transmitted light through DSSC glazing can be calculated from the measured SPD transmittance, D65 spectral power distribution and the color matching functions as shown in Fig. 4 (CIE Publication, 1988).

$$X = \sum_{380\,nm}^{780\,nm} D_{65}(\lambda)\tau(\lambda)\bar{x}(\lambda)\Delta\lambda \quad (2)$$

$$Y = \sum_{380\,nm}^{780\,nm} D_{65}(\lambda)\tau(\lambda)\bar{y}(\lambda)\Delta\lambda \quad (3)$$

$$Z = \sum_{380\,nm}^{780\,nm} D_{65}(\lambda)\tau(\lambda)\bar{z}(\lambda)\Delta\lambda \quad (4)$$

Chromacity coordinate (x, y) can be calculated by below equation

$$x = \frac{X}{X+Y+Z} \text{ and } y = \frac{Y}{X+Y+Z}$$

CCT was calculated from McCamy's equation (McCamy, 1992)

$$CCT = 449n^3 + 3525n^2 + 6823.3n + 5520.33 \quad (5)$$

where $n = \frac{(x-0.3320)}{(0.1858-y)}$ and x, y chromacity coordinate

Step 2 for CRI calculation

For CRI evaluation tristimulus values of the light transmitted by the glazing and reflected by each of eight test colors (i = 1 to8) are given by where test color are defined by their spectral reflectance $\beta_i(\lambda)$.

$$X_{t,i} = \sum_{380\,nm}^{780\,nm} D_{65}(\lambda)\tau(\lambda)\beta_i(\lambda)\bar{x}(\lambda)\Delta\lambda \quad (6)$$

$$Y_{t,i} = \sum_{380\,nm}^{780\,nm} D_{65}(\lambda)\tau(\lambda)\beta_i(\lambda)\bar{y}(\lambda)\Delta\lambda \quad (7)$$

Table 2
Fabricated DSSC based on different electrode thickness and electrical conversion efficiency.

Device name	TiO_2 layer thickness (μm)	Electrical conversion efficiency (%)
L2	3.5	2.51
L3	6	4.49
L4	8	5.02
L5	10	5.93
L6	12	5.15
L7	14	3.24

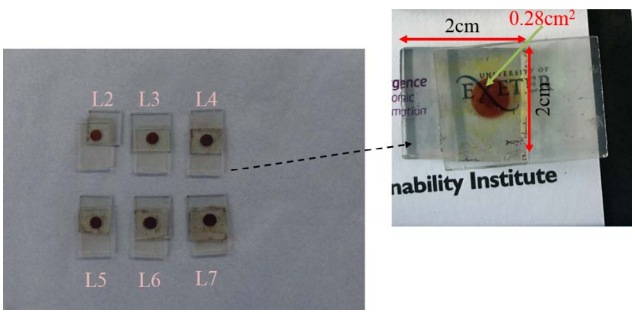

Fig. 2. Fabricated six DSSC and exploded view of one DSSC.

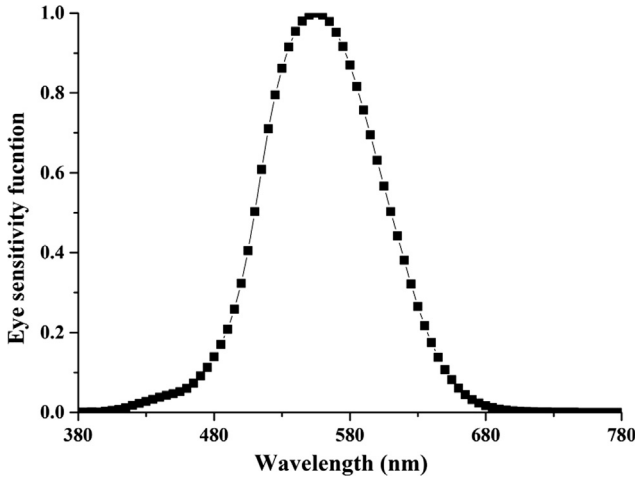

Fig. 3. Standardization curve of eye sensitivity to wavelength of light (CIE 15, 2004).

$$Z_{t,i} = \sum_{380\,\mathrm{nm}}^{780\,\mathrm{nm}} D_{65}(\lambda)\tau(\lambda)\beta_i(\lambda)\overline{z}(\lambda)\Delta\lambda \tag{8}$$

Trichromatic coordinates u_t and v_t for the transmitted light were determined from

$$u_t = \frac{4X}{X + 15Y + 3Z} \text{ and } v_t = \frac{6X}{X + 15Y + 3Z} \tag{9}$$

Each test color for the light transmitted and then reflected by the test color i is thus given by

$$u_{t,i} = \frac{4X_{t,i}}{X_{t,i} + 15Y_{t,i} + 3Z_{t,i}} \text{ and } v_{t,i} = \frac{6X_{t,i}}{X_{t,i} + 15Y_{t,i} + 3Z_{t,i}} \tag{10}$$

Trichromatic coordinate correction after distortion by chromatic adaptation is provided by

$$u'_{t,i} = \frac{10.872 + 0.8802\frac{c_{t,i}}{c_t} - 8.2544\frac{d_{t,i}}{d_t}}{15.518 + 3.2267\frac{c_{t,i}}{c_t} - 2.0636\frac{d_{t,i}}{d_t}}, \tag{11}$$

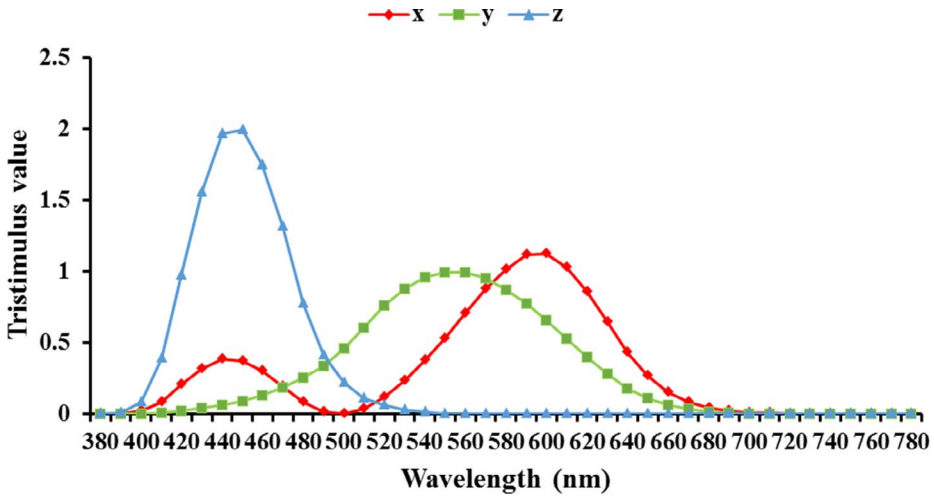

Fig. 4. The spectral response of the color matching functions $\overline{x}(\lambda)$,$\overline{y}(\lambda)$,$\overline{z}(\lambda)$.

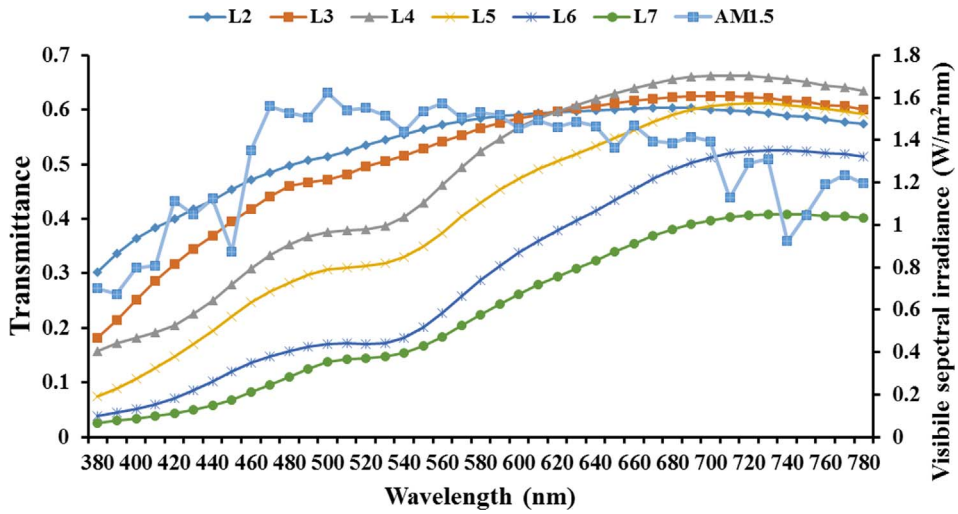

Fig. 5. Normal-hemispherical spectral transmittance of DSSC cells. Transmission was compared with AM 1.5 solar spectrum. Only the visible part of the spectrum [380–780 nm] is relevant for this work.

Table 3
Luminous transmission of different DSSC glazing.

Device name	TiO_2 layer thickness (μm)	Efficiency [%]	Luminous transmission (%) (380–780 nm)
L2	3.5	2.51	53
L3	6	4.49	50
L4	8	5.02	44
L5	10	5.93	37
L6	12	5.15	25
L7	14	3.24	19

$$v'_{t,i} = \frac{5.520}{15.518 + 3.2267\frac{c_{t,i}}{c_t} - 2.0636\frac{d_{t,i}}{d_t}} \tag{12}$$

where c_t and d_t for transmitted light and $c_{t,i}$ and $d_{t,i}$ for each light transmitted and then reflected by test color are calculated from

$$c_t = \frac{4 - u_t - 10v_t}{v_t},\ d_t = \frac{1.708v_t + 0.404 - 1.481u_t}{v_t} \tag{13}$$

$$c_{t,i} = \frac{4 - u_{t,i} - 10v_{t,i}}{v_{t,i}},\ d_{t,i} = \frac{1.708v_{t,i} + 0.404 - 1.481u_{t,i}}{v_{t,i}} \tag{14}$$

Colour space system $W^*_{t,i}$, $U^*_{t,i}$, $V^*_{t,i}$ are given by

$$W^*_{t,i} = 25\left(\frac{100Y_{t,i}}{Y_t}\right)^{1/3} - 17 \tag{15}$$

$$U^*_{t,i} = 13W^*_{t,i}(u'_{t,i} - 0.1978) \tag{16}$$

$$V^*_{t,i} = 13W^*_{t,i}(V'_{t,i} - 0.3122) \tag{17}$$

The total distortion (color difference between the color coordinates determined for the same test color samples illuminated by test and the reference illuminants) ΔE_i is determined from

$$\Delta E_i = \sqrt{(U^*_{t,i} - U^*_{r,i})^2 + (V^*_{t,i} - V^*_{r,i})^2 + (W^*_{t,i} - W^*_{r,i})^2} \tag{18}$$

The special color rendering index R_i for each color sample is given by

$$R_i = 100 - 4.6\Delta E_i \tag{19}$$

The general color rendering index (CRI) is thus given by

$$CRI = \frac{1}{8}\sum_{i=1}^{8} R_i \tag{20}$$

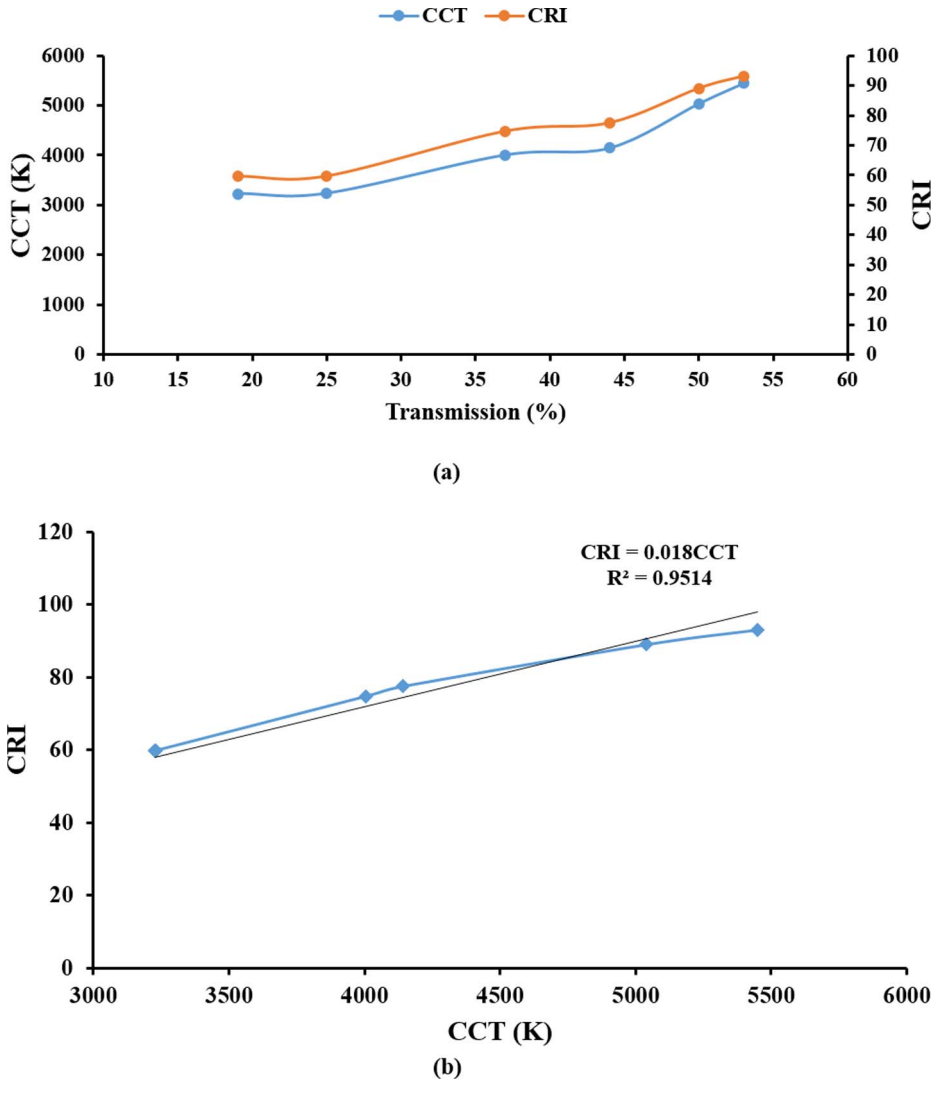

Fig. 6. (a) Variation of CCT and CRI with transmission, (b) correlation between CCT and CRI for different DSSC cells for glazing application.

Table 4
CRI and CCT values for different electrode thickness of DSSC glazing.

Device name	CRI	CCT (K)
L2	93	5449.96
L3	88	5038.53
L4	77	4142.72
L5	74	4004.13
L6	59.74	3230.87
L7	59.67	3226.09

4. Results & discussion

4.1. Luminous transmittance of DSSC

Fig. 5 shows the normal-hemispherical transmittance of the six different DSSC glazing samples. Luminous transmission was calculated using Eq. (1). Table 3 summarises the luminous transmission for different DSSC glazing. Number of dyes attached to the thick electrode is higher than thin electrode, which absorb higher amount of light and introduce low transmittance (Yoon et al., 2011). However, no linear relation was found between DSSC transmission and efficiency. Too thick TiO_2 layers (samples L6 11.9 μm, and L7 13.6 μm) increase the length of the electron pathways, and thus decrease fill factor, open circuit voltage and in extreme cases even short circuit current (Desilvestro, 2008) which reduce the overall electrical efficiency of the solar cell.

4.2. CCT and CRI for DSSC glazing

Fig. 6a shows the variation of CCT and CRI with transmission and Fig. 6b illustrates the correlation of CCT and CRI for different transparent DSSCs by varying electrode thickness. CCT was calculated using Eq. (5) and CRI was calculated from Eq. (20). Different CCT and CRI values for different DSSC glazings are listed in Table 4. A strong linear correlation was found between CCT and CRI for DSSC glazing. It can be concluded that higher achievable CRI also offers higher CCT. For indoor light condition, a CCT from 3000 K to 5300 K and CRI of more than 80 are generally required (D'Andrade and Forrest, 2004). To realize a high CRI, a DSSC should have an enough broad spectral coverage, but it leads to a high CCT, which is not suitable for indoor comfort. L2 (3.5 μm thick electrode) and L3 (6 μm thick electrode) devices offer better CRI and CCT compared to other layers.

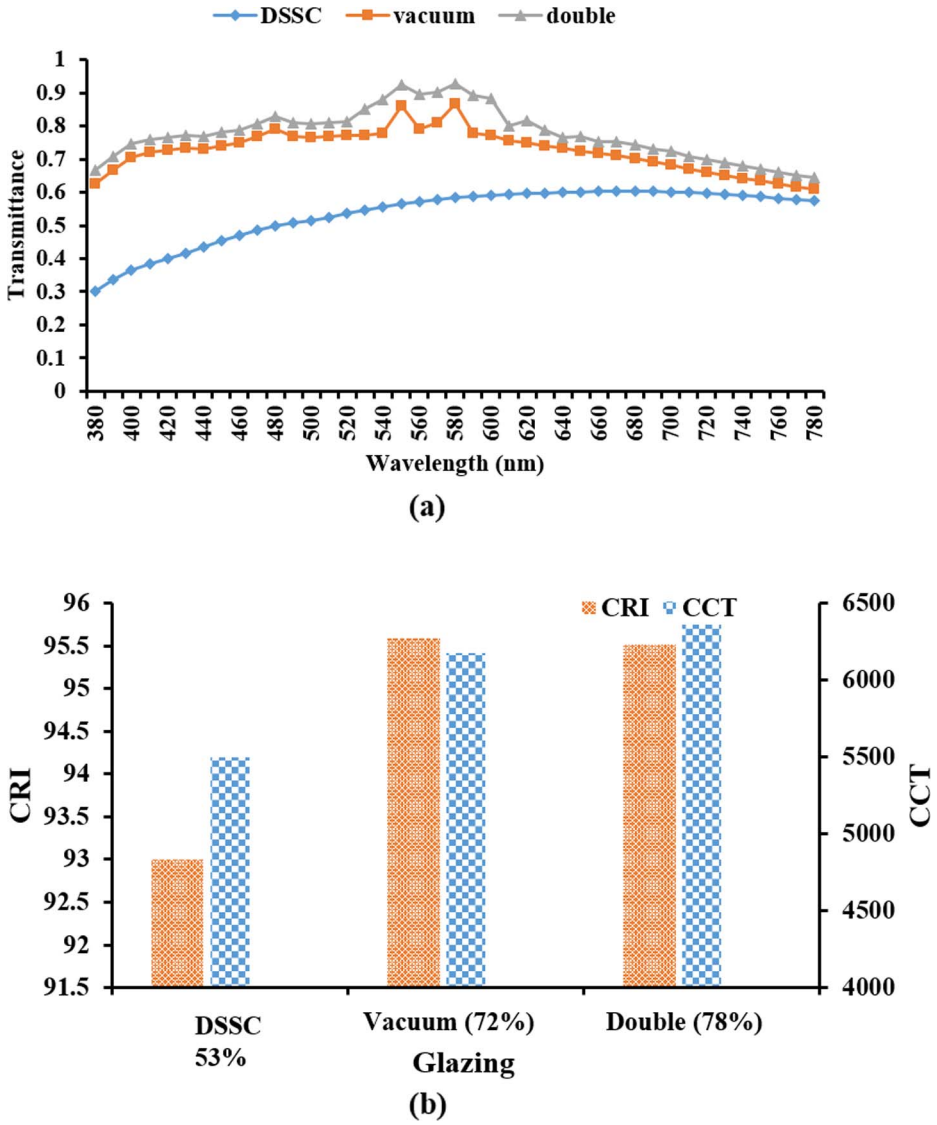

Fig. 7. (a) Normal-hemispherical spectral transmittance in the visible (380–780 nm) range, (b) comparison of CCT and CRI for DSSC (53%), vacuum glazing and double-glazing.

Table 5
CCT and CRI for 53% transparent DSSC, vacuum, double-glazing.

Type of glazing	CCT (K)	CRI	Transmission (%)
DSSC	5449.9	93	53
Vacuum	6178	95.59,	72
Double	6360	95.51	78

4.3. CCT & CRI comparison of DSSC with vacuum and double glazing

Fig. 7a shows the normal hemispherical transmission of 53% transparent DSSC glazing, double and vacuum glazing. Vacuum glazing consists vacuum between two glass panes and potential to reduce heat loss in northern climatic conditions (Ghosh et al., 2016c, 2017c). Double-glazing is a widely available glazing technology for building window applications (Chow et al., 2011; Gil-Lopez and Gimenez-Molina, 2013). Thus, these two glazing systems were considered in this work to compare the behaviour of adaptive DSSC glazing. Presence of low emission coating in the double and vacuum glazing influenced to decrease transmission after 600 nm whereas DSSC showed increasing of transmission after 600 nm. Fig. 7b indicates the CCT and CRI for 53% transparent DSSC, 72% transparent vacuum glazing and 78% transparent double-glazing. DSSC glazing has 45% less transmission compared to double glazing and 35% less than vacuum glazing, however, CRI only compromise 2.7% less compared to both glazing. It indicates that CRI depends more on the wavelength dependent spectral values than one single transmittance value. Table 5 shows the CCT and CRI for these three different types of glazings.

5. Conclusions

CCT and CRI for DSSC glazing were calculated. Different transparent DSSCs were fabricated using different TiO_2 electrode thickness. It was found that 53% and 50% transparent DSSC offered achievable CRI and CCT. Results of 53% transparent DSSC was compared with vacuum and double-glazing. Vacuum and double-glazing, which have higher transparency than DSSC, offered only 2.7% higher CRI and CCT values near to overcast sky. DSSC glazing is a potential device as it offers small-scale clean electricity with amicable light color for occupant. 53% transparent DSSC offered best CRI and CCT, however, 37% transmission offered best efficiency. It can be concluded that DSSC glazing higher than 50% transparent is a potential glazing system for new or retrofit window, as they possess allowable CRI and CCT.

Acknowledgment

This work has been partially supported by research project ‘Joint UK-India Clean Energy Centre (JUICE)’ which is funded by the RCUK's Energy Programme (contract no: EP/P003605/1). The projects funders were not directly involved in the writing of this article. In support of open access research, all underlying article materials (data, models) can be accessed upon request via email to the corresponding author.

References

Al Dakheel, J., Tabet Aoul, K., 2017. Building applications, opportunities and challenges of active shading systems: a state-of-the-art review. Energies 10, 1672. http://dx.doi.org/10.3390/en10101672.

Berginc, M., Opara Krašovec, U., Jankovec, M., Topič, M., 2007. The effect of temperature on the performance of dye-sensitized solar cells based on a propyl-methyl-imidazolium iodide electrolyte. Sol. Energy Mater. Sol. Cells 91, 821–828. http://dx.doi.org/10.1016/j.solmat.2007.02.001.

Bommel, W.J.M.Van, van der Beld, J.G., 2004. Lighting for work: a review of visual and biological effects. Light. Res. Technol. 36, 255–269.

Cannavale, A., Hörantner, M., Eperon, G.E., Snaith, H.J., Fiorito, F., Ayr, U., Martellotta, F., 2017. Building integration of semitransparent perovskite-based solar cells: Energy performance and visual comfort assessment. Appl. Energy 194, 94–107. http://dx.doi.org/10.1016/j.apenergy.2017.03.011.

Chain, C., Dumortier, D., Fontoynont, M., 2001. Consideration of daylight’s colour. Energy Build. 33, 193–198. http://dx.doi.org/10.1016/S0378-7788(00)00081-5.

Chow, T.T., Li, C., Lin, Z., 2011. Thermal characteristics of water-flow double-pane window. Int. J. Therm. Sci. 50, 140–148. http://dx.doi.org/10.1016/j.ijthermalsci.2010.10.006.

CIE 15, 2004. Technical Report: Colorimetry. Color. 3rd Ed. 552, 24. doi: ISBN 3 901 906 33 9.

CIE Publication, 75-1988, 1988. Spectral Luminous Efficiency Functions Based Upon Brightness Matching for Monochromatic Point Sources with 2° and 10° Fields ISBN 3900734119.

Cuce, E., 2016. Toward multi-functional PV glazing technologies in low/zero carbon buildings: Heat insulation solar glass – latest developments and future prospects. Renew. Sustain. Energy Rev. 60, 1286–1301. http://dx.doi.org/10.1016/j.rser.2016.03.009.

D’Andrade, B.W., Forrest, S.R., 2004. White organic light-emitting devices for solid-state lighting. Adv. Mater. 16, 1585–1595.

Davis, R.G., Grinthner, D.N., 1990. Correlated color temperature, illuminance level, and the Kruithof curve. J. Illum. Eng. Soc. 19, 27–38.

Desilvestro, H., 2008. What physical factors affect current-voltage characteristics of dye solar cells? Dye. Tech. Lit. 1–16.

En, B.S., 2001. Glass in building—determination of the emissivity.

Favoino, F., Overend, M., Jin, Q., 2015. The optimal thermo-optical properties and energy saving potential of adaptive glazing technologies. Appl. Energy 156, 1–15. http://dx.doi.org/10.1016/j.apenergy.2015.05.065.

Ghosh, A., 2014. Multifunctional Glazing System-Solution for Modern Smart Glazing, pp. 1–8.

Ghosh, A., Mallick, T.K., 2018. Evaluation of colour properties due to switching behaviour of a PDLC glazing for adaptive building integration. Renew. Energy 120, 126–133. http://dx.doi.org/10.1016/j.renene.2017.12.094.

Ghosh, A., Norton, B., 2017a. Durability of switching behaviour after outdoor exposure for a suspended particle device switchable glazing. Sol. Energy Mater. Sol. Cells 163, 178–184. http://dx.doi.org/10.1016/j.solmat.2017.01.036.

Ghosh, A., Norton, B., 2017b. Interior colour rendering of daylight transmitted through a suspended particle device switchable glazing. Sol. Energy Mater. Sol. Cells 163, 218–223. http://dx.doi.org/10.1016/j.solmat.2017.01.041.

Ghosh, A., Norton, B., Duffy, A., 2017a. Effect of atmospheric transmittance on performance of adaptive SPD-vacuum switchable glazing. Sol. Energy Mater. Sol. Cells 161, 424–431. http://dx.doi.org/10.1016/j.solmat.2016.12.022.

Ghosh, A., Norton, B., Duffy, A., 2017b. Effect of sky conditions on light transmission through a suspended particle device switchable glazing. Sol. Energy Mater. Sol. Cells 160, 134–140. http://dx.doi.org/10.1016/j.solmat.2016.09.049.

Ghosh, A., Norton, B., Duffy, A., 2017c. Effect of sky clearness index on transmission of evacuated (vacuum) glazing. Renew. Energy 105, 160–166. http://dx.doi.org/10.1016/j.renene.2016.12.056.

Ghosh, A., Norton, B., Duffy, A., 2016a. Measured thermal performance of a combined suspended particle switchable device evacuated glazing. Appl. Energy 169, 469–480. http://dx.doi.org/10.1016/j.apenergy.2016.02.031.

Ghosh, A., Norton, B., Duffy, A., 2016b. Behaviour of a SPD switchable glazing in an outdoor test cell with heat removal under varying weather conditions. Appl. Energy 180, 695–706. http://dx.doi.org/10.1016/j.apenergy.2016.08.029.

Ghosh, A., Norton, B., Duffy, A., 2016c. Measured thermal & daylight performance of an evacuated glazing using an outdoor test cell. Appl. Energy 177, 196–203. http://dx.doi.org/10.1016/j.apenergy.2016.05.118.

Ghosh, A., Norton, B., Duffy, A., 2016d. Daylighting performance and glare calculation of a suspended particle device switchable glazing. Sol. Energy 132, 114–128. http://dx.doi.org/10.1016/j.solener.2016.02.051.

Ghosh, A., Norton, B., Duffy, A., 2016e. First outdoor characterisation of a PV powered suspended particle device switchable glazing. Sol. Energy Mater. Sol. Cells 157, 1–9. http://dx.doi.org/10.1016/j.solmat.2016.05.013.

Ghosh, A., Norton, B., Duffy, A., 2015. Measured overall heat transfer coefficient of a suspended particle device switchable glazing. Appl. Energy 159, 362–369. http://dx.doi.org/10.1016/j.apenergy.2015.09.019.

Ghosh, A., Norton, B., Mallick, T.K., 2018a. Daylight characteristics of a polymer dispersed liquid crystal switchable glazing. Sol. Energy Mater. Sol. Cells 174, 572–576. http://dx.doi.org/10.1016/j.solmat.2017.09.047.

Ghosh, A., Mallick, T.K., 2018b. Evaluation of optical properties and protection factors of a PDLC switchable glazing for low energy building integration. Sol. Energy Mater. Sol. Cells 176, 391–396. http://dx.doi.org/10.1016/j.solmat.2017.10.026.

Gil-Lopez, T., Gimenez-Molina, C., 2013. Influence of double glazing with a circulating water chamber on the thermal energy savings in buildings. Energy Build. 56, 56–65. http://dx.doi.org/10.1016/j.enbuild.2012.10.008.

Gong, J., Liang, J., Sumathy, K., 2012. Review on dye-sensitized solar cells (DSSCs): fundamental concepts and novel materials. Renew. Sustain. Energy Rev. 16, 5848–5860. http://dx.doi.org/10.1016/j.rser.2012.04.044.

Gong, J., Sumathy, K., Qiao, Q., Zhou, Z., 2017. Review on dye-sensitized solar cells (DSSCs): advanced techniques and research trends. Renew. Sustain. Energy Rev. 68, 234–246. http://dx.doi.org/10.1016/j.rser.2016.09.097.

Gong, X., Wang, S., Moses, D., Bazan, G.C., Heeger, A.J., 2005. Multilayer polymer light-emitting diodes: white-light emission with high efficiency. Adv. Mater. 17, 2053–2058.

Grätzel, M., 2003. Dye-sensitized solar cells. J. Photochem. Photobiol. C Photochem. Rev. 4, 145–153. http://dx.doi.org/10.1016/S1389-5567(03)00026-1.

Gunde, M.K., Krašovec, U.O., Platzer, W.J., 2005. Color rendering properties of interior lighting influenced by a switchable window. J. Opt. Soc. Am. A 22, 416. http://dx.doi.org/10.1364/JOSAA.22.000416.

Hee, W.J., Alghoul, M.A., Bakhtyar, B., Elayeb, O., Shameri, M.A., Alrubaih, M.S., Sopian,

K., 2015. The role of window glazing on daylighting and energy saving in buildings. Renew. Sustain. Energy Rev. 42, 323–343. http://dx.doi.org/10.1016/j.rser.2014.09.020.

Hernández-Andrés, J., Lee, R.L., Romero, J., 1999. Calculating correlated color temperatures across the entire gamut of daylight and skylight chromaticities. Appl. Opt. 38, 5703–5709. http://dx.doi.org/10.1364/AO.38.005703.

Ito, S., Murakami, T.N., Comte, P., Liska, P., Grätzel, C., Nazeeruddin, M.K., Grätzel, M., 2008. Fabrication of thin film dye sensitized solar cells with solar to electric power conversion efficiency over 10%. Thin Solid Films 516, 4613–4619. http://dx.doi.org/10.1016/j.tsf.2007.05.090.

Jelle, B.P., Hynd, A., Gustavsen, A., Arasteh, D., Goudey, H., Hart, R., 2012. Fenestration of today and tomorrow: a state-of-the-art review and future research opportunities. Sol. Energy Mater. Sol. Cells 96, 1–28. http://dx.doi.org/10.1016/j.solmat.2011.08.010.

Kang, J.G., Kim, J.H., Kim, J.T., 2013. Performance evaluation of DSC windows for buildings. Int. J. Photoenergy 2013. http://dx.doi.org/10.1155/2013/472086.

Kang, M.G., Park, N.G., Park, Y.J., Ryu, K.S., Chang, S.H., 2003. Manufacturing method for transparent electric windows using dye-sensitized TiO_2 solar cells. Sol. Energy Mater. Sol. Cells 75, 475–479. http://dx.doi.org/10.1016/S0927-0248(02)00202-7.

Kumara, N.T.R.N., Lim, A., Lim, C.M., Petra, M.I., Ekanayake, P., 2017. Recent progress and utilization of natural pigments in dye sensitized solar cells: a review. Renew. Sustain. Energy Rev. 78, 301–317. http://dx.doi.org/10.1016/j.rser.2017.04.075.

Luo, M.R., 2011. The quality of light sources. Color. Technol. 127, 75–87.

Lynn, N., Mohanty, L., Wittkopf, S., 2012. Color rendering properties of semi-transparent thin-film PV modules. Build. Environ. 54, 148–158. http://dx.doi.org/10.1016/j.buildenv.2012.02.010.

Mardaljevic, J., 2014. How to Maintain Neutral Daylight Illumination with SageGlass ® Electrochromic Glazing (whitepaper) 18.

Mathew, S., Yella, A., Gao, P., Humphry-Baker, R., Curchod, B.F.E., Ashari-Astani, N., Tavernelli, I., Rothlisberger, U., Nazeeruddin, M.K., Grätzel, M., 2014. Dye-sensitized solar cells with 13% efficiency achieved through the molecular engineering of porphyrin sensitizers. Nat. Chem. 6, 242–247. http://dx.doi.org/10.1038/nchem.1861.

McCamy, C.S., 1992. Correlated color temperature as an explicit function of chromaticity coordinates. Color Res. Appl. 17, 142–144. http://dx.doi.org/10.1002/col.5080170211.

Miyazaki, T., Akisawa, A., Kashiwagi, T., 2005. Energy savings of office buildings by the use of semi-transparent solar cells for windows. Renew. Energy 30, 281–304. http://dx.doi.org/10.1016/j.renene.2004.05.010.

Morini, M., Corrao, R., 2017. Energy optimization of BIPV glass blocks: a multi-software study. Energy Procedia 111, 982–992. http://dx.doi.org/10.1016/j.egypro.2017.03.261.

Ng, P.K., Mithraratne, N., 2014. Lifetime performance of semi-transparent building-integrated photovoltaic (BIPV) glazing systems in the tropics. Renew. Sustain. Energy Rev. 31, 736–745. http://dx.doi.org/10.1016/j.rser.2013.12.044.

Niu, X., Ma, L., Yao, B., Ding, J., Tu, G., Xie, Z., Wang, L., 2006. White polymeric light-emitting diodes with high color rendering index. Appl. Phys. Lett. 89, 213508.

O'Regan, B., Gratzel, M., 1991. A low-cost, high efficiency solar cell based on dye-sensitized colloidal TiO_2 films. Nature 353, 737–740.

Parisi, A., Pernice, R., Andò, A., Cino, A.C., Franzitta, V., Busacca, A.C., 2017. Electro-optical characterization of ruthenium-based dye sensitized solar cells: A study of light soaking, ageing and temperature effects. Optik (Stuttg). 135, 227–237. http://dx.doi.org/10.1016/j.ijleo.2017.01.100.

Park, K.E., Kang, G.H., Kim, H.I., Yu, G.J., Kim, J.T., 2010. Analysis of thermal and electrical performance of semi-transparent photovoltaic (PV) module. Energy 35, 2681–2687. http://dx.doi.org/10.1016/j.energy.2009.07.019.

Rezaei, S.D., Shannigrahi, S., Ramakrishna, S., 2017. A review of conventional, advanced, and smart glazing technologies and materials for improving indoor environment. Sol. Energy Mater. Sol. Cells 159, 26–51. http://dx.doi.org/10.1016/j.solmat.2016.08.026.

Richhariya, G., Kumar, A., Tekasakul, P., Gupta, B., 2017. Natural dyes for dye sensitized solar cell: a review. Renew. Sustain. Energy Rev. 69, 705–718. http://dx.doi.org/10.1016/j.rser.2016.11.198.

Senthilarasu, S., Peiris, T.A.N., Garc, J., Wijayantha, K.G.U., 2012. Preparation of nano-crystalline TiO_2 electrodes for flexible dye-sensitized solar cells: influence of mechanical compression. J. Phys. Chem. C 116, 19053–19061.

Shalini, S., Balasundara Prabhu, R., Prasanna, S., Mallick, T.K., Senthilarasu, S., 2015. Review on natural dye sensitized solar cells: operation, materials and methods. Renew. Sustain. Energy Rev. 51, 1306–1325. http://dx.doi.org/10.1016/j.rser.2015.07.052.

Sharma, S., Siwach, Bulkesh, Ghoshal, S.K., Mohan, D., 2017. Dye sensitized solar cells: from genesis to recent drifts. Renew. Sustain. Energy Rev. 70, 529–537. http://dx.doi.org/10.1016/j.rser.2016.11.136.

Shen, K., Li, Q., Wang, D., Yang, R., Deng, Y., Jeng, M.J., Wang, D., 2016. CdTe solar cell performance under low-intensity light irradiance. Sol. Energy Mater. Sol. Cells 144, 472–480. http://dx.doi.org/10.1016/j.solmat.2015.09.043.

Skandalos, N., Karamanis, D., 2015. PV glazing technologies. Renew. Sustain. Energy Rev. 49, 306–322. http://dx.doi.org/10.1016/j.rser.2015.04.145.

Sudan, M., Tiwari, G.N., 2016. Daylighting and energy performance of a building for composite climate: an experimental study. Alexandria Eng. J. 55, 3091–3100. http://dx.doi.org/10.1016/j.aej.2016.08.014.

Sudan, M., Tiwari, G.N., 2014. Energy matrices of the building by incorporating daylight concept for composite climate – an experimental study. J. Renew. Sustain. Energy 6. http://dx.doi.org/10.1063/1.4898364.

Sudan, M., Tiwari, G.N., Al-Helal, I.M., 2015. A daylight factor model under clear sky conditions for building: an experimental validation. Sol. Energy 115, 379–389. http://dx.doi.org/10.1016/j.solener.2015.03.002.

Upadhyaya, H.M., Senthilarasu, S., Hsu, M.H., Kumar, D.K., 2013. Recent progress and the status of dye-sensitised solar cell (DSSC) technology with state-of-the-art conversion efficiencies. Sol. Energy Mater. Sol. Cells 119, 291–295. http://dx.doi.org/10.1016/j.solmat.2013.08.031.

Webb, A.R., 2006. Considerations for lighting in the built environment: non-visual effects of light. Energy Build. 38, 721–727. http://dx.doi.org/10.1016/j.enbuild.2006.03.004.

Wei, Z., Bobbili, P.R., Senthilarasu, S., Shimell, T., Upadhyaya, H.M., 2014. Design and optimisation of process parameters in an in-line CIGS evaporation pilot system. Surf. Coat. Technol. 241, 159–167. http://dx.doi.org/10.1016/j.surfcoat.2013.10.033.

Yoon, S., Tak, S., Kim, J., Jun, Y., Kang, K., Park, J., 2011. Application of transparent dye-sensitized solar cells to building integrated photovoltaic systems. Build. Environ. 46, 1899–1904. http://dx.doi.org/10.1016/j.buildenv.2011.03.010.